Integrated geophysical imaging of the Alalobeda geothermal field (Ethiopia)

Daniele Rizzello[1], Egidio Armadillo[2], Massimo Verdoya[2], Claudio Pasqua[2,3], Solomon Kebede[4], Andarge Mengiste[4], Neway Abera[5]

[1]Tellus sas (Italy), [2]University of Genoa (Italy), [3] ELC-Electroconsult, Milano S.p.A. (Italy), [4]Geological Survey of Ethiopia, [5]Ethiopian Electric Company

geodriz75@yahoo.it

Keywords: Magnetotellurics, Gravity, Geothermics, Integrated interpretation.

ABSTRACT

A geothermal exploration project was founded by the Icelandic International Development Agency (ICEIDA) and the Nordic Development Fund (NDF), with the aim of assessing the geothermal resources of Alalobeda (Ethiopia). The Alalobeda geothermal system is located along the western margin of the Tendaho Graben, where the NW tectonic structures of the graben intersect the NNE trending Main Ethiopian Rift (MER) lineaments yielding intense rock fracturation. An integrated geophysical survey was carried out during in 2014-15, over an area of about 140 km2. The geophysical campaign comprised 123 coincident magnetotelluric and time domain soundings and 300 gravity stations. 2-D and 3-D gravimetric models inferred two NW trending major normal faults hidden by the graben sediment infill. Between them, the basaltic bedrock shows a structure made by second order horsts and grabens. The 3-D electrical resistivity model reveals that the basalts cropping out and the sediments covering the bedrock in the graben depression show exceptionally low resistivities (sometimes lower than 1 Ohm m). In this general frame, three NNE trending fracture zones were inferred by their enhanced conductivity in the 3D model. The fracture zones are located in the shoulder sector of the NW trending Tendaho Graben, where the topography and the structural observations indicate the presence of NNE trending MER normal faults. All the three inferred fracture zones are put into evidence by more resistive deeper anomaly, interpreted as high-temperature alteration, and a shallower very conductive layer, interpreted as a low-temperature clay cap. The fracture zones do not continue towards the plain and appear to be limited by the NW Tendaho Graben main normal fault. The resistivity pattern appears compatible with a main fluid path trending NNE along the MER fracture zones while orthogonal flow is likely driven by the intersecting NW Tendaho faults.

1. INTRODUCTION

The African countries that are located along the East African Rift System (EARS) have the largest geothermal potential of the continent, estimated as about 15,000 MWe. However, only Kenya and Ethiopia have so far installed a capacity of about 217 MWe (Teklemariam Zemedkun, 2011); at the moment, the only geothermal plant in Ethiopia is located in the Mt Aluto area (Lakes District, Central Main Ethiopian Rift).

This paper presents the results of recent geophysical study aimed at improving the knowledge of the geothermal resources in Alalobeda, located in the Tendaho Graben (TG), Afar Region (Ethiopia), in view of the possible production of geothermal energy. The geophysical campaign consisted of MT-TEM soundings and gravity measurements. The acquired MT data were integrated with the results of a previous, campaign, carried out by Geological Survey of Ethiopia in 2013.

2. GEOLOGICAL SETTING

The Alalobeda geothermal field is located in the Afar Depression, Ethiopia, at the western flank of the Tendaho Graben (Figure 1). The Depression is a diffuse triple junction located where the Red Sea, Gulf of Aden and Main Ethiopian rifts converge. This structure originated by the separation of the Arabian, Nubian and Somalian tectonic plates. The plate boundary divergence started 25 Ma ago, when the Arabian and the Nubian plates began to separate, but an effective triple junction was formed about 11 Ma ago, when the northward propagating Main Ethiopian Rift reached the Afar Depression (Corti, 2009).

Primarily, Afar is a region of active extensional tectonics and strike slip faulting plays a secondary role in the overall tectonic setting (Abbate 1995). The triple junction is interpreted as due to a mantle plume impinging on the base of the continental lithosphere; this feature could justify the anomalous thermal regime and the upwelling of the Ethiopian plateaus. The persistence of a plume can also explain the lithosphere thinning, demonstrated by seismological

studies in this region (Dugda et al, 2007). Hammond et al. (2011) estimated the crustal thickness, from seismological data, to be about 26 km in Central Afar and 16 km in Northern Afar.

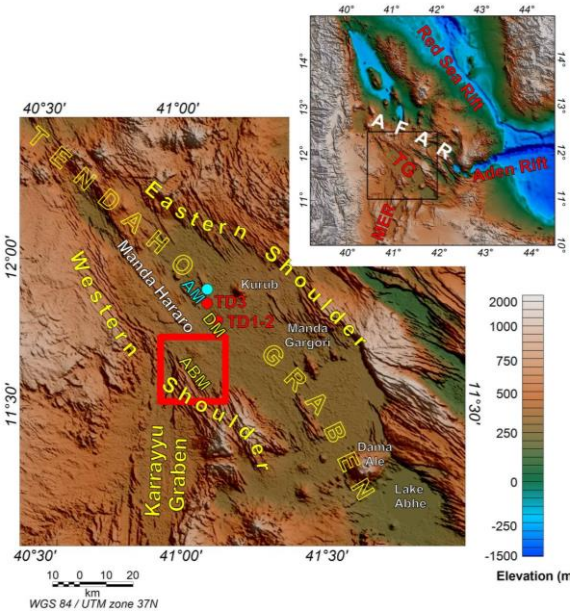

Figure 1: Map of the Afar Region and main structural features: Tendaho Graben (TG); Main Ethiopian Rift (MER). Geothermal manifestations: ABM-Alalobeda, AM-Ayrobera, DM-Dubti; Deep exploratory wells: TD-1, -2 and -3. Red square is the survey area (see also Fig. 2).

Basaltic magmatism is widely diffused throughout the Afar region; it began 30 Ma ago with the eruption of flood basalts (Corti, 2009). These rocks are now lying in the plateaus surrounding the Afar Depression. The continuous tectonic activity favoured the magmatic activity, and several fissural and central volcanic complexes are widespread across the region. The more recent and diffused volcanic event occurred from 4 to 1.6 Ma, producing the Afar Stratoid Basalts (ASS), that constitute the present-day rock-basement. Crustal partial melt was inferred from several geophysical studies. Didana et al. (2015) reported results of MT resistivity modeling, from which high conductivity layers are identified at relatively shallow depths (<10 km). Now, the most active area, with contemporary magmatic and seismic activity is the Manda-Hararo fissural volcano (Fig. 1), which is active since 3 Ma ago and the last eruption is dated 2009 (Ferguson et al., 2010).

The enhanced tectonic activity and thermal regime favour the occurrence of several possible geothermal areas in the TG, such as Dubti, Ayrobera and Alalobeda (Fig. 1). Some information about the deep structure of the TG can be obtained from three deep wells drilled in the 90's, whose main results are shown in Figure 2. The (compact) Afar Stratoids were encountered in the Dubti area at about 1400 and 1200 m depth in the wells TD-1 and TD-2, respectively. The stratigraphy consists of a sedimentary cover overlying the ASS basalts. Sediments are of lacustrine origin, with some intercalations of more recent basalts and minor pyroclastic layers. No stratigraphic information is available for the Alalobeda area. We therefore assume that the stratigraphic sequence in Alalobeda is similar to Dubti, with the possible differences in sediment thickness because of the vicinity to the graben shoulder.

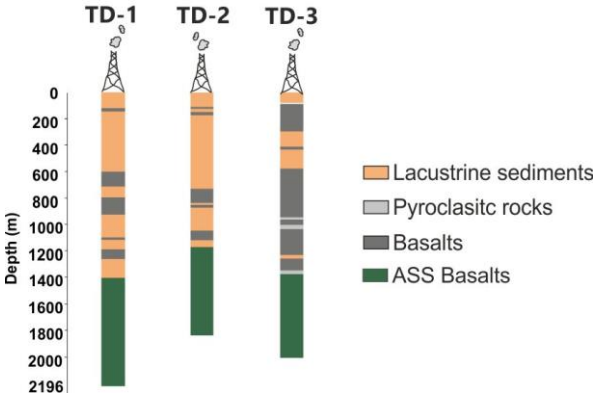

Figure 2: stratigraphy of wells TD-1, TD-2, TD-3 (after Aquater, 1996).

The Alalobeda area is characterized by the presence of several geothermal manifestations, such as fumaroles and hot springs (with temperature up to 98°C). Thermal springs are located in correspondence of the graben master fault (see Fig. 3). A geochemical study indicates a maximum reservoir temperature of 220°C (ELC, 2015). In Alalobeda, the intersection between the NW-trending Tendaho Graben and the NNE-trending Karrayu Graben (Fig. 1) produces widespread fracturing, as can also be observed from the surface geology. This condition is a key factor for the development of a possible geothermal reservoir.

3. GEOPHYSICAL SURVEY

The survey area (Fig. 1) is partly located in the sedimentary cover of the TG and partly over the graben western shoulder, constituted by the ASS basalts. The area was densely covered with MT/TEM and gravity stations, and its extent is about 140 km^2 (Fig. 3). Three-hundred gravity data were acquired according to a square grid, with a lower density grid in the western sector. More than one-hundred MT measurements were carried out. Station spacing was about 1.5 km, except near the Alalobeda geothermal springs, where it was reduced to about 750 m. with some exceptions when site accessibility was difficult or strong topographic effects had to be avoided.

3.1 Gravity

Gravity data were acquired in combination with differential GPS positioning. Measurements were executed starting and ending at a base station for daily drift correction. The average density evaluation to be determined for the Bouguer and topographic correction was estimated by means of a dual approach: the Nettleton method (Nettleton, 1939) and 3-D

forward modelling. To apply the Nettleton technique, 10 profiles were chosen over the ASS basalts. The average value of the density estimated for each profile was 2450 kg m^{-3}.

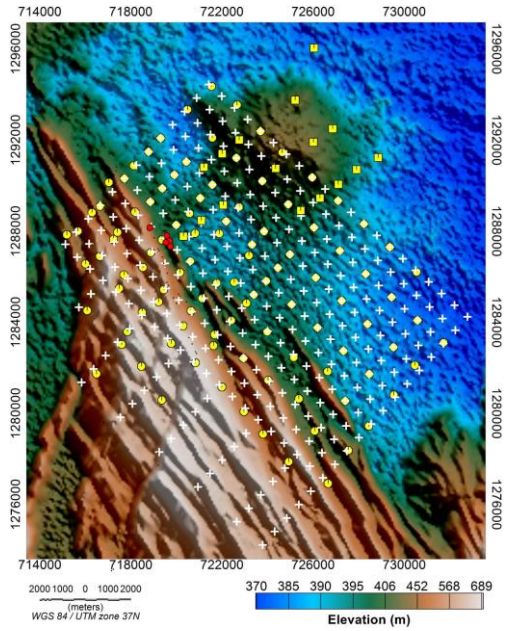

Figure 3: Position of the geophysical survey stations. Yellow circles - MT stations of the 2014 campaign; yellow squares - MT stations of 2013; white crosses - gravity stations. Red circles - Alalobeda hot springs.

A second independent estimation of the ASS density was obtained from a forward modelling approach. We restricted our analysis to the basaltic mountainous area. Then we computed the Free Air Anomaly due to the topography for different homogeneous density, and compared it with the measured values. The misfit between the calculated and measured gravity data was evaluated by minimising the root mean square (RMS) error; an optimal density value of 2520 kg m^{-3} was found. The final density of 2485 kg m^{-3} adopted for the Bouguer and terrain correction is an average of the two methods.

The value of the complete Bouguer anomaly (-23.038 mGal) obtained for the western sector of the ASS basalts was assumed as the regional gravity field. In this part of the investigated area, the rather uniform gravity anomaly can be interpreted as due to the absence of density lateral variations.

Figure 4 shows the residual gravity anomaly map, obtained after subtracting the regional field from the Bouguer anomaly. The map shows i) a wide positive anomaly that follows the graben shoulder, with a maximum value of +4.3 mGal and ii) a large negative belt in the plain, with a minimum value of -5.1 mGal. The negative anomaly is associated with the low-density sedimentary infill, while the positive anomaly may be associated with a positive density contrast source. The main positive anomaly belt can be further divided into three areas (AH1, AH2a and AH2b), whereas in the negative anomaly one can distinguish two areas, AL1 and AL2. In particular, in AL1, linear trends (L1 and L2) can be clearly inferred.

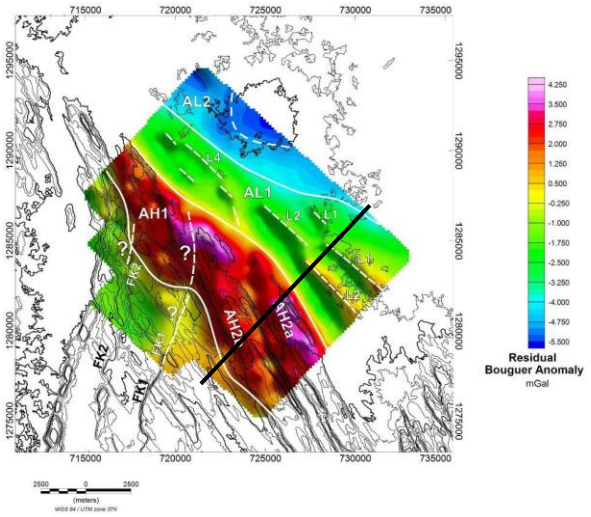

Figure 4: residual Bouguer Anomaly map. The positive anomaly is divided into three areas AH1, AH2a and AH2b. The negative anomaly is divided into two subsectors AL1 and AL2. AL1 denote the zone with linear trends. The black line indicates profile T16.

The possible origin of the higher density body may be related to mineral alterations in the ASS basalts. The same 2-D modelling carried for other profiles allowed an evaluation of the body extent.

Figure 5 shows an example of 2-D forward modelling along profile T16 (see Fig. 4 for location). We found that the anomaly can be explained by a denser zone in the ASS, located between 500 and 2000 m depth, i.e. at elevations between 0 and 1500 m b.s.l.; moreover, the AH2a and AH2b anomalies are adequately explained by the model with small basins filled with low-density sediments.

The possible origin of the higher density body may be related to mineral alterations in the ASS basalts.

The residual Bouguer map and the 2-D modelling provides some clues about the presence of second order grabens and horst buried beneath the sedimentary cover (Fig. 5), that are related to the L1 and L2 structures. In order to depict the bedrock surface and to get a more accurate imaging of such structures, we performed a 3-D gravity inversion of the residual Bouguer anomaly. The model was defined by a number of stacked surface grids, with assigned density distributions specified for the layer below each surface. The inversion adjusted each surface shape until a minimum misfit data was reached. The used surfaces were the topography, the surface of the bedrock and that of the anomaly depicted by 2-D forward modelling. The surface of the bedrock beneath the sediments was set as the topography shifted 100 m downward. We assigned to the

sediments a density contrast of -450 kg/m^3, and +300 kg/m^3 to the anomalous body in the ridge.

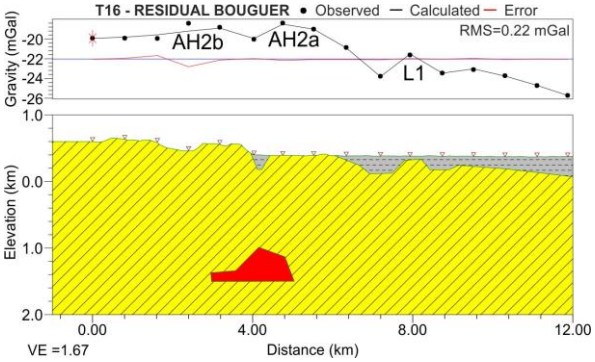

Figure 5: 2-D forward gravity modelling along profile T16. Yellow: ASS basalts (0 kg/m^3); grey: sedimentary cover (-450 kg/m^3); red: anomalous body (+450 kg/m^3). AH2a, AH2b and L1 as in Figure 4.

The obtained ASS bedrock surface elevation is shown in Fig. 6. It reveals a horst-graben structure hidden by the sedimentary cover of the graben. The structures are similar to the ones emerging from the sediments and flanking the graben shoulder.

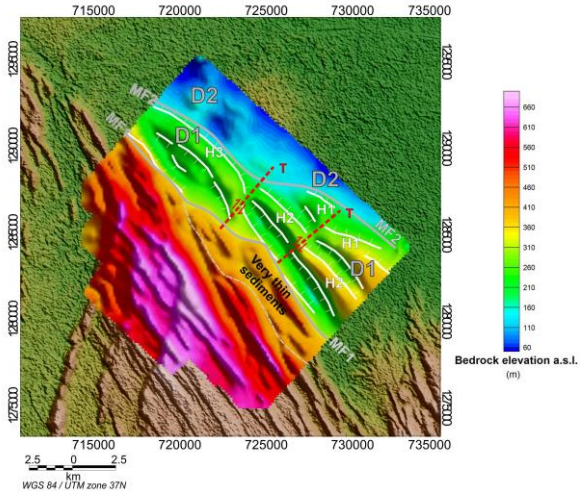

Figure 6: map of the ASS bedrock elevation a.s.l. obtained from the 3-D gravimetric inversion. White lines: horst-graben structures mapped along the maxima of the topography horizontal gradient. MF1-MF2: main graben normal faults that define structural domains D1 and D2.

The main faults controlling the bedrock structures can be put into evidence by analysing the maxima of the horizontal gradient of the bedrock topography (Fig. 6). The main fault system that originates the main graben depression is marked by MF1 (heavy grey line). A second main fault system MF2 (dashed grey line) divides the main depression into two sub-regions D1 and D2. In the region D1, several horst-graben structures are visible (white lines, horsts labelled by H1-H3) trending NW. These horst-graben structures appear shifted by two inferred transversal lineaments (red lines) interpreted as strike slip faults.

3.2 MT and TEM results

The data from MT stations were acquired in the 1000-0.0001 Hz range by means of three equipments. One station was permanently located at a reference site located in Ayrobera, at a distance of about 20 km from the survey area (Fig. 1). The record length of acquisitions varied from 17.5 to 70.2 hours, with a mean of 26.3. The MT impedance and geomagnetic tipper were estimated by a combination of the remote reference technique (Gamble et al., 1979) and the robust MT processing (Sutarno, 2008). Thanks to the impedance estimation method and to the very low noise in the survey area, we obtained MT impedances of outstanding quality (see the example in Fig. 7).

To correct for the MT static shift effect, a parallel TEM (Transient Electromagnetic) campaign was carried out, including also the MT locations of the 2013 survey, whose data were processed together with the data recorded in the new campaign. Shift factors were computed through joint inversion of MT phase and TEM apparent resistivity data. From this procedure, two apparent resistivity correcting factors (s_{xy}, s_{yx}) were calculated for each station and used to correct the MT impedance, with the relation

$$Z_c = C\,Z_d = \begin{pmatrix} \sqrt{s_{xy}} & 0 \\ 0 & \sqrt{s_{yx}} \end{pmatrix} \begin{pmatrix} Z_{xx} & Z_{xy} \\ Z_{yx} & Z_{yy} \end{pmatrix} \qquad [1]$$

In eq. [1], $\boldsymbol{Z_d}$ and $\boldsymbol{Z_c}$ are the distorted and corrected impedance, respectively, while $\boldsymbol{C}$ is the correction matrix. We implicitly assumed that the static distortion can be modelled by a simple linear relationship.

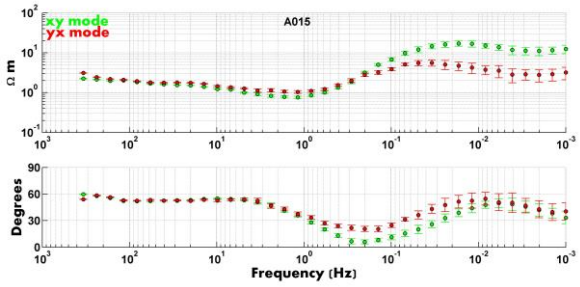

Figure 7: example of MT data (station A015). Top: apparent resistivity; bottom: phase.

The final dataset of 123 MT stations was employed to perform a 3-D inversion by means of the ModEM software (Egbert & Kelbert, 2012; Kelbert et al., 2014) with additions for parallel computing described by Meqbel (2009). We inverted the full unrotated and static shift-corrected impedance tensor (Z), jointly with tipper (T_z), using 19 periods in the range between 0.003 s and 1000 s. We assigned error floors of 5 % of $\left|\left(Z_{xy}^2\, Z_{yx}^2\right)^{1/2}\right|$ to the four complex impedance tensor components. A constant value of 0.03 was used as an

error floor for the tipper components. Some heavily biased or scattered data points were manually discarded after inspection.

The 3-D grid used consists of 90 by 92 cells in x - and y directions, extending from -25 to +25 km in E-W (y) direction and from -25 to +26 km in N-S (x) direction. In the central portion, where the MT sites are located, the horizontal cell size is 300 m. Figure 8 shows a view of the vertical mesh used in the central portion of the model.

The MT 3-D inversion was carried out with different initial models, in order to validate the final model being interpreted. Thus, inversion was carried out starting with (i) a 50 Ohm m homogeneous medium, (ii) a 10 Ohm m homogeneous medium and (iii) with the resistivity distribution resulting by the linear interpolation of smooth 1-D models. The same smoothing coefficient was applied to all the inversions. All the three inversion runs gave very similar final results and misfit.

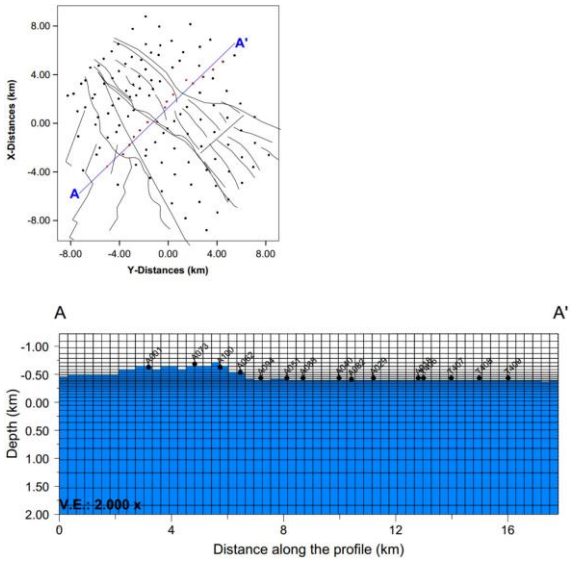

Figure 8: vertical meshing in the central portion of the 3-D model. Location of the profile top and position of MT stations (dots) are given in the inset above.

Figure 9 shows the results of the 3-D inverted model derived from the initial 1D interpolated model. The tectonic lineaments inferred from the gravity study are also shown. The resistivity contrast between the graben basin and the basaltic ridge sector can be clearly noticed from the slices at 400 and -200 m a.s.l. The sediment conductive layer (S-CL) is in some areas highly conductive (<0.5 Ohm m). This is in agreement with the results by Armadillo et al. (2014), showing similar values deduced from 2D MT profiles located South of Dubti. According to Aquater (1996), such a low resistivity may be due to high-salinity fluids, and/or the presence of a clayey matrix in the sedimentary cover. Two conductive anomalies appear in the ASS basalts, namely at 400 m (ASS-CL1) and -200 m (ASS-CL2). They show a very low resistivity of about 1 Ohm m. The origin of the ASS-CL2 anomaly seems to be related to the MER-trending structures visible from topography, and to deeper anomalous zones (FZ1-FZ3). These deep anomalous zones are visible between -800 and -1500 m a.s.l., and show a resistivity of about 5-30 Ohm m. The ASS-CL1 anomaly may be originated by shallow strong hydrothermal alteration.

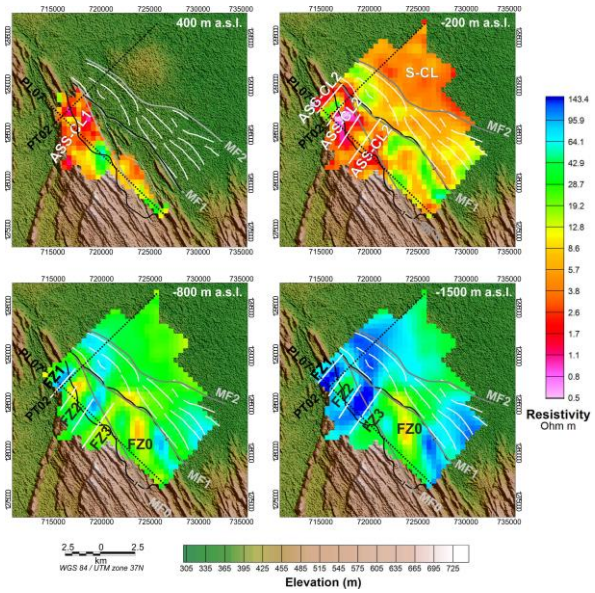

Figure 9: horizontal slices of resistivity from the MT 3-D inversion model. Dashed black lines show the location of the resistivity profiles. Other symbols in text.

Another important anomaly (FZ0) is visible at larger depth (from -600 to -1500 m a.s.l.). It presents a N-S trend and may be caused by enhanced hydrothermal alteration focussed along a large and deep structural discontinuity.

Figure 10 depicts two vertical resistivity profiles extracted from the 3-D inversion. The first (PT02) is perpendicular and the second (PL07) is parallel to the Alalobeda master faults (see Fig. 9 for their location). The graben steps are well depicted by the resistivity distribution of the conductive sedimentary cover and track the gravimetric bedrock profile. On the base of the gravimetric bedrock mapping, it can also be noticed that the conductive layer S-CL comprises the sediments and a low-resistivity layering in the underlying ASS basalts. Probably, this layering represents an altered portion of the bedrock. In the basaltic ridge sector (left side of the profile), the ASS-CL1 and ASS-CL2 conductive anomaly are well discernible. Their resistivity is about 1 Ohm m, and as far as we know, it is the lowest resistivity ever measured over the ASS basalts. Moreover, in PT02, the gravity anomaly >1 mGal finds a correspondence with the maximum thickness of alteration in the ASS basalts constituting the graben shoulder.

The profile PL07 clearly shows the three conductive anomalies visible in Figure 9 (altogether labelled as ASS-CL2). These anomalies are located in prosecution of the MER faults. Below each ASS-CL2

anomaly, the resistivity bedrock (RB) shows a correspondent deepening. We interpret these features as generated by enhanced hydrothermal alteration focussed along the permeable fracture zones FZ1-FZ3. High-temperature clays cause the deepening of the resistive bedrock at depth, while low-temperature clays generate the stronger ASS-CL2 anomalies at shallower depth. Note that the FZ0 zone deepens much more than the other deepens, but does not exhibits a corresponding (low-temperature) conductive cap.

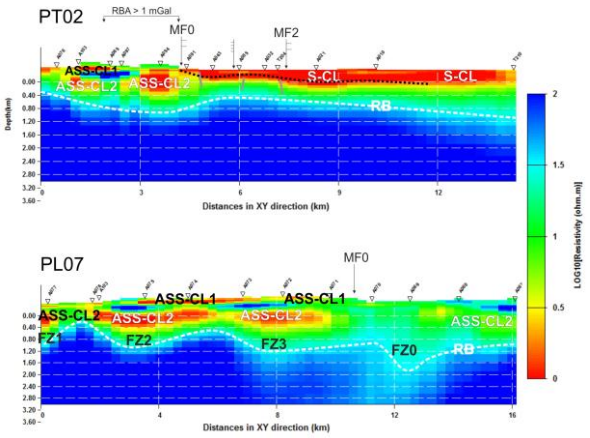

Figure 10: resistivity sections PT02 and PL07 obtained from the MT 3-D inversion results. The bedrock resistivity, arbitrarily defined by a value of 30 Ohm m, is shown (white dashed line, labelled RB). The position of the tectonic lineaments inferred from the gravity study is indicated with black arrows. The black dotted line is the gravimetric bedrock. Grey lines indicate the normal faults. The gravimetric bedrock, deduced from the 3-D gravity inversion is marked with the black dashed line. Position of the gravimetric positive anomaly (RBA >1 mGal) is also shown along the profile PT02.

4. DISCUSSION

The joint interpretation of the gravity and magnetotelluric results can help to decipher the structure of the Alalobeda geothermal field. The integration of the two methods can be done by means of suitable synoptic maps.

The resistivity horizontal slice at -800 m a.s.l. is shown in Figure 11 together with the lineaments inferred from the gravity study. The topography of the top of the anomalous body delineated by the gravity 3-D inversion is also displayed as black contour lines. It can be noticed that the body with anomalous density can be associated with a diffuse conductive zone (5-10 Ohm m) located at depth in the ridge sector between the MF0 and MF1 main faults. The resistivity of this zone may indicate a relatively high-temperature alteration of the ASS basalts. This observation confirms that the anomalous density body can be explained as an altered volume in the ASS basalts.

Variations in the ASS basalts resistivity (Fig. 9) suggest different alteration grades. If we assume that deep alteration in the ASS basalts can be qualitatively represented by the vertical variations of the 30 Ohm iso-resistive surface, a deepening this surface indicates that alteration penetrates at larger higher depth and vice-versa.

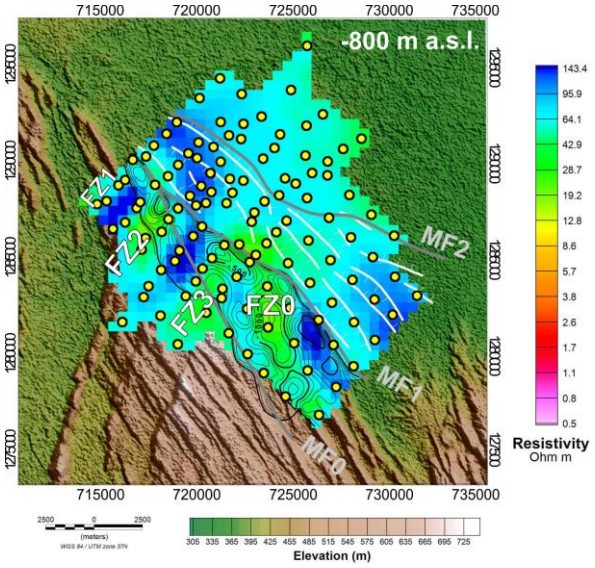

Figure 11: horizontal resistivity slice at - 800m a.s.l. from 3D inversion of MT data. Yellow circles are positions of MT stations.

The alteration map is shown in Figure 12, together with the gravimetric lineaments. Four main alteration zones (AZ0-AZ3) can be identified. The AZ0 alteration zone extends over the MF1 main fault and reaches the plain, while AZ1-AZ3 are limited to the NE by the MF1 main fault system. The AZ1-AZ3 zones are compatible with a fluid path trending NNE along the MER fracture zones, while orthogonal flow is likely driven by the intersecting NW-trending Tendaho faults. From a comparison with Figure 3, we notice that the Alalobeda hot springs are located close to the intersection of the FZ2 and the MF1 main fault. The AZ0 zone trends N-S and is not related to shallow faults revealed by gravity or topography; it may be related to geothermal fluid upflow. Globally AZ0 and AZ3 seem to underline an alteration band orthogonal to the graben shoulder, and extending northeastwards. The southeastern limit of this alteration band well agrees with the strike slip lineament inferred from gravity.

5. CONCLUSIONS

The combination of gravimetric and magnetotelluric surveys and the use of advanced interpretation techniques, are useful tools to understand the structure of high-temperature geothermal systems

The use of these techniques in the Alalobeda area revealed the presence of several alteration zones. Most of them are compatible with a geothermal fluid flow towards N-NE, along fracture zones related to the

Main Ethiopian Rift. Orthogonal flow is likely driven by the intersecting NW Tendaho faults. The Alalobeda hot springs are located near the intersection of one of these fracture zones with a major Tendaho Graben fault, buried beneath the sediments and inferred with the gravity survey. The Main Ethiopian Rift lineaments seem then to play an important role in the geothermal fluid circulation of Alalobeda.

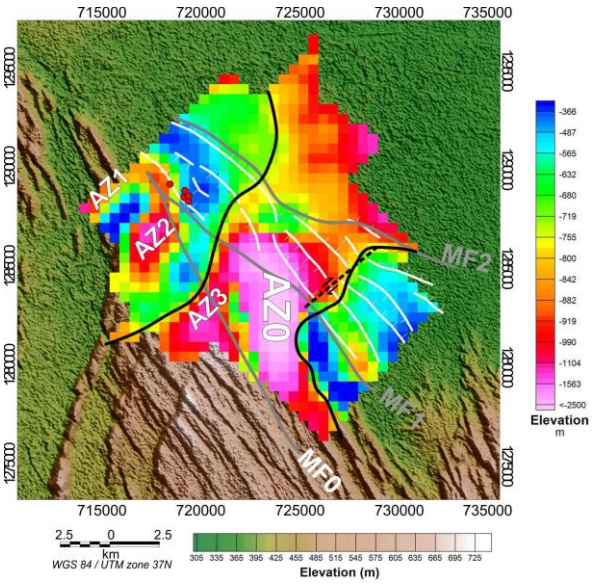

Figure 12: Elevation a.s.l. of the 30 Ohm iso-resistive surface. Down-doming of the surface is interpreted here as indicative of greater alteration in the ASS basalts. The Alalobeda hot springs are marked by red circles.

The low-temperature clay caps of the fracture zones show very low resistivities, namely < 1 Ohm m; these values are the lowest ever measured over the ASS basalts. The joint interpretation of gravity and resistivity information strongly supports the hypothesis that the bulk density of the ASS basalts can be increased by the high-temperature alteration.

REFERENCES

Abbate, E., Passerini, P., Zan, L.: Strike-slip faults in a rift area: a transect in the Afar Triangle, East Africa. *Tectonophysics*, 241, (1995), 67-97.

Aquater: *Tendaho Geothermal Project, Final Report, Volume 1*. Aquater S.p.A., San Lorenzo in Campo, Italy, (1996), 324 pp.

Armadillo, E., Rizzello, D., Stimac, J.: Geophysical Assessment of the Tendaho Area. *Unpublished Report to UNEP* (2014).

Corti, G.: Continental rift evolution: From rift initiation to incipient break-up in the Main Ethiopian Rift, East Africa. *Earth-Science Reviews*, 96, (2009), 1-53.

Didana, Y., L., Thiel, S., Heinson, G.: Three dimensional conductivity model of the Tendaho High Enthalpy Geothermal Field, NE Ethiopia. *Journal of Volcanology and Geothermal Research*, 290, (2015), 53-62.

Dugda, M.T., Nyblade, A.A., Julia, J.: Thin Lithosphere Beneath the Ethiopian Plateau Revealed by a Joint Inversion of Rayleigh Wave Group Velocities and Receiver Functions. *J. Geophys. Res.*, 112, (2007), B08305.

ELC-Electroconsult: Alalobeda Geochemical report. (2015)

Egbert, G.D., Kelbert, A.: Computational recipes for electromagnetic inverse problems. *Geophys. J. Int.*, 189, (2012), 251-267.

Ferguson, D., J., Barnie, T.D., Pyle, D.M., Oppenheimer, C., Yirgu, G., Lewi, E., Kidane, T., Carn, S., Hamling, I.: Recent rift-related volcanism in Afar, Ethiopia. *Earth and Planetary Science Letters*, 292, (2010), 409-418.

Gamble, T.D., Goubau, W.M., Clarke, J.: Magnetotellurics with a remote magnetic reference. *Geophysics*, 44, (1979), 53-68.

Hammond, J.O.S., Kendall, J.M., Stuart, G.W., Keir, D., Ebinger, C., Ayele, A. and Belachew, M.: The nature of the crust beneath the Afar triple junction: Evidence from receiver functions. *Geochemistry Geophysics Geosystems*, 12, (12), (2011), Q12004.

Kelbert A, Meqbel N, Egbert GD, Tandon K.: ModEM: A modular system for inversion of electromagnetic geophysical data. *Computers & Geosciences*, 66, (2014), 40-53.

Meqbel, N.: The electrical conductivity structure of the Dead Sea Basin derived from 2D and 3D inversion of magnetotelluric data. *PhD thesis*, Free University of Berlin, Berlin, Germany, (2009).

Sutarno, D.: Constrained robust estimation of magnetotelluric impedance functions based on a bounded-influence regression M-estimator and the Hilbert transform. *Nonlin. Processes Geophys.*, 15, (2008), 287-293.

Teklemariam Zemedkun, M.: Overview of geothermal resource exploration and development in the East African Rift System. *Presented at Short Course VI on Exploration for Geothermal Resources, organized by UNU-GTP, GDC and KenGen*, Lake Bogoria and Lake Naivasha, Kenya, (2011).